1994

Transonic Inviscid Disc Flows in the Schwarzschild Metric – I

Menas Kafatos
Chapman University, kafatos@chapman.edu

Ruixin Yang
George Mason University

Recommended Citation
Kafatos, M., Yang, R. (1994) Transonic Inviscid Disc Flows in the Schwarzschild Metric – I, *Monthly Notices of the Royal Astronomical Society*, 268:925-937. doi: 10.1093/mnras/268.4.925

Transonic Inviscid Disc Flows in the Schwarzschild Metric – I

Mon. Not. R. Astron. Soc. **268,** 925–937 (1994)

Transonic inviscid disc flows in the Schwarzschild metric – I

Menas Kafatos[1,2] and Ruixin Yang[1]

[1] *Institute for Computational Sciences & Informatics, George Mason University, Fairfax, VA 22030-4444, USA*
[2] *Department of Physics, George Mason University, Fairfax, VA 22030-4444, USA*

Accepted 1994 January 19. Received 1993 October 28; in original form 1992 December 3

ABSTRACT

The coupled hydrodynamic equations governing equatorial flows applicable to inviscid disc accretion in the Schwarzschild metric are solved analytically and numerically. Here, we concentrate on the transonic solutions, that represent physically allowed accretion on to black holes. A polytropic equation linking gas pressure and density is assumed, and solutions are obtained for different conditions, such as isothermal and adiabatic gas flows. The dependence of those solutions on the angular momentum is explored. Under certain conditions, when there exist multiple possible sonic points, the numerical simulation automatically zeros in to the unique transonic solution passing through one of the sonic points.

Key words: accretion, accretion discs – black hole physics – hydrodynamics.

1 INTRODUCTION

Accretion discs around black holes are generally postulated as the energy source of active galactic nuclei (AGN) and galactic X-ray sources, such as Cygnus X-1 (Ling et al. 1987) and the galactic source 1E 1740.7 – 2942 (Sunyaev et al. 1991). Ever since the seminal paper on standard alpha-disc theory by Shakura & Sunyaev (1973), accretion disc theory has been applied to a variety of high-energy sources. Although the standard α-disc model predicts that discs would become radiation-pressure-dominated near the black hole, such disc regions become unstable to thermal and secular perturbations (Lightman & Eardley 1974). Shapiro, Lightman & Eardley (1976) in turn proposed that two-temperature ion, pressure-dominated regions would form near the black hole. Such regions have been postulated by Eilek & Kafatos (1983), and more recently by Becker & Kafatos (1994), as the sources of high-energy radiation, including γ-rays in the range 1 MeV–1 GeV, from such sources as the quasar 3C 279 (Hartman et al. 1992).

The basic reason why an accretion disc around a compact object is likely to form is that the accreting gas has rather high specific angular momentum, and so cannot accrete directly on to the black hole (Shakura & Sunyaev 1973; Kafatos 1988; Frank, King & Raine 1992). For a given angular momentum, a circular orbit has least energy, so that dissipation processes would tend to circularize the orbits of particles. Although circular Keplerian orbits are expected to be the rule, deviations may take place near the black hole.

Accretion on to black holes may not actually follow the usual steady inflow process assumed in α-discs. Accretion on to black holes may always be a transonic phenomenon, with the transonic radius close to the black hole if the accretion occurs in a thin-disc configuration (Liang & Thompson 1980; Abramowicz & Zurek 1981; Abramowicz & Kato 1989).

The existence of critical points (sonic points where the inflow velocity equals the sound speed) in the flows on to black holes has been investigated by a variety of authors under different conditions. The existence of critical points in spherical, steady-state, optically thick accretion on to black holes was investigated by Flammang (1982). Adiabatic flows and the resultant transonic solutions in Schwarzschild metric were investigated by Lu (1985), and the more general problem of finding sonic surfaces in adiabatic flows in a stationary axisymmetric space–time was investigated by Anderson (1989). Analytic solutions, however, are generally not obtainable, and also have not been compared to numerical solutions in previous works.

As a first step, we have developed the relativistically correct continuity and Euler's equations in the Schwarzschild metric, ignoring viscosity terms. Viscous effects would, of course, need to be included in a realistic scenario of accretion. However, because, after 20 years of work by many people, the origin of viscosity still eludes us, and because we are interested in comparing numerical solutions with analytic solutions, the simplest possible case is justified as a first step. In an infinitesimally thin disc, or for motion near the equatorial plane, the fluid equations assume particularly simple forms in the radial and azimuthal directions. Here, we present the results for the resulting flows, assuming that a polytropic relationship holds between the gas pressure and

density. By assuming a polytropic equation, we can treat the whole problem without the need to include the energy balance equation. Radiation processes would, of course, need to be considered in a realistic scenario of accretion flows (cf. Thorne 1981; Thorne, Flammang & Żytkow 1981), particularly if the flow is optically thick, in which case radiative transfer would need to be included. If the flows near the horizon result in optically thin conditions, as Shapiro, Lightman & Eardley (1976) assumed, the inclusion of relativistic radiative transfer is not necessary in a first approximation. Finally, we are ignoring the effects of production of electron–positron pairs (Liang 1979; Svensson 1984; Kusunose & Takahara 1985). Such effects are discussed elsewhere (Becker & Kafatos 1994).

In the following sections, the one-dimensional fully relativistic hydrodynamic equations for inviscid flows are given first. Then, the analytical and numerical solutions to the governing equations are discussed. The emphasis of this work is on the velocity fields (profiles), and on variations of the important properties, such as the locations of sonic points and accretion rates, with angular momentum. A special case with multiple possible sonic points is also studied.

In subsequent papers we will examine the possibility of shocks, motions off the orbital plane for which $u^\theta \neq 0$, and flows in the full Kerr metric.

2 THE GOVERNING EQUATIONS AND THE METHODS FOR SOLUTIONS

2.1 Equations and parameters

The problem we consider here is steady gas accretion on to black holes, taking into account the relativistic fluid equations written in spherical coordinates. For steady flows along the equatorial plane applicable to a thin disc, the four-velocity (u^r, u^θ, u^ϕ and u^t) in the Schwarzschild metric has only two independent components, u^r and u^ϕ. The only independent variable is the radial distance from the black hole r, since the azimuthal and time dependences are dropped due to the symmetry and steady-flow assumptions; moreover, the angle θ is limited to a given constant value, and we take here $\theta = \pi/2$ at the equatorial (or, more appropriately, disc) plane. The basic coupled fluid equations in this case are written as

$$u^r \frac{\mathrm{d}u^r}{\mathrm{d}r} = \left(r - \frac{3GM}{c^2}\right)(u^\phi)^2 - \frac{GM}{r^2} - \left(1 - \frac{2GM}{c^2 r}\right)\frac{c^2}{w}\frac{\mathrm{d}p}{\mathrm{d}r} - \frac{(u^r)^2}{w}\frac{\mathrm{d}p}{\mathrm{d}r} \tag{1}$$

and

$$2ru^\phi + r^2\frac{\mathrm{d}u^\phi}{\mathrm{d}r} = -r^2 u^\phi \frac{1}{w}\frac{\mathrm{d}p}{\mathrm{d}r}, \tag{2}$$

while the continuity equation becomes

$$nu^r r^2 = \text{constant}. \tag{3}$$

Instead of using the energy equation, we assume a gas-dominated pressure p, and a polytropic relation

$$p = Kn^\gamma = nk(T_\mathrm{e} + T_\mathrm{i}). \tag{4}$$

In the above, $w = \varepsilon + p$, and is the enthalpy per unit volume; $\varepsilon = nk(\lambda_\mathrm{e} T_\mathrm{e} + \lambda_\mathrm{i} T_\mathrm{i}) + n(m_\mathrm{p} + m_\mathrm{e})c^2$, and is the proper internal energy density (Shapiro 1973, 1974); T_i and T_e are the temperatures of ions and electrons, respectively, and $n = n_\mathrm{i} = n_\mathrm{e}$ is the particle number density for a fully ionized pure hydrogen gas. The constants m_p and m_e denote the rest masses of protons and electrons, and k, c and G used below have the same meaning as commonly used in the literature. Here, the assumption is made that the increase of the mass of the black hole, M, due to the accretion process itself, can be ignored; the parameter M, therefore, is a constant. The limiting values of λ_i and λ_e are

$$\lambda_\mathrm{e} = \begin{cases} \frac{3}{2} & \text{when } \dfrac{kT_\mathrm{e}}{m_\mathrm{e}c^2} \ll 1, \\ 3 & \text{when } \dfrac{kT_\mathrm{e}}{m_\mathrm{e}c^2} \gg 1, \end{cases}$$

and

$$\lambda_\mathrm{i} = \begin{cases} \frac{3}{2} & \text{when } \dfrac{kT_\mathrm{i}}{m_\mathrm{p}c^2} \ll 1, \\ 3 & \text{when } \dfrac{kT_\mathrm{i}}{m_\mathrm{p}c^2} \gg 1. \end{cases}$$

The $(1/w)(\mathrm{d}p/\mathrm{d}r)$ term in the above equations can be reduced and expressed in terms of u^r only. Therefore the ordinary differential equations (ODEs) describing u^r and u^ϕ, respectively, can be written in u^r and u^ϕ only. We can then make the two resultant equations dimensionless by choosing $r_\mathrm{g} = GM/c^2$ and c as the length and velocity scales. Defining the dimensionless quantities $X = r/r_\mathrm{g}$, $u = u^r/c$ and $v = u^\phi r/c$, we obtain the dimensionless equations

$$\frac{\mathrm{d}u}{\mathrm{d}X} = \frac{N}{D} \tag{5}$$

and

$$\frac{\mathrm{d}v}{\mathrm{d}X} = Bv\left(\frac{1}{u}\frac{\mathrm{d}u}{\mathrm{d}X} + \frac{2}{X}\right) - \frac{v}{X}, \tag{6}$$

where the numerator N in (5) has the form

$$N = (X-3)\frac{v^2}{X^2} - \frac{1}{X^2} + \frac{2B}{X}\left(1 - \frac{2}{X} + u^2\right), \tag{7}$$

and the denominator D is

$$D = (1-B)\,u - \frac{B}{u}\left(1 - \frac{2}{X}\right). \tag{8}$$

The parameter B, defined as $(\mathrm{d}p/\mathrm{d}n)(n/w)$, which equals the square of the local sound speed, is obtained as

$$B = \frac{\gamma}{(1+\lambda_\mathrm{i}) + \dfrac{(\lambda_\mathrm{e} - \lambda_\mathrm{i})\,T_\mathrm{e}}{T_\mathrm{e} + T_\mathrm{i}} + A^{-1}}, \tag{9}$$

where

$$A \equiv \frac{k(T_\mathrm{e} + T_\mathrm{i})}{(m_\mathrm{p} + m_\mathrm{e})c^2}. \tag{10}$$

Here, we will consider the case with $T_e \ll T_i$ ('hot' disc), and the case with $T_e = T_i$ and $\lambda_e = \lambda_i$ ('cool' disc). Therefore the term $(\lambda_e - \lambda_i)\, T_e/(T_e + T_i)$ can always be ignored, and the parameter B can be rewritten as

$$B = \frac{\gamma}{(1+\lambda) + A^{-1}}, \tag{11}$$

with $\lambda = \lambda_i = \lambda_e$. In the isothermal situation, the temperature is constant, and therefore the sound speed ($\sqrt{B}$) is constant.

Equations (5) and (6) describe the steady inviscid gas accretion on to a black hole. The emphasis of this work is to solve these equations in order to investigate the effects of the angular momentum of the accreting gas. To find the solutions to the governing equations, one needs to determine the parameters in the equations and to provide suitable conditions. Since we are handling ODEs here, we need only specify the boundary conditions at a certain location, say X_0. At X_0, we should fix u_0, v_0 and $(T_e + T_i)_0$ to integrate the governing equations. According to the values of the temperature, we will consider hot discs, $(T_e + T_i)_0 \sim 10^{13}$ K, $A_0 = 1$, and 'cooler' discs, $(T_e + T_i)_0 \ll 10^{13}$ K, $A_0 \ll 1$. The value of the parameter λ is either 3 for hot discs or 3/2 for cool discs. We will consider two polytropic processes: the isothermal case, in which $\gamma = 1$, and the adiabatic case, in which $\gamma = (\lambda+1)/\lambda$.

From the continuity equation and the polytropic relation, and knowing the velocity distribution, one may find the other state variables, namely temperature, density and pressure, by the relations

$$T_e + T_i = (T_e + T_i)_0 \left(\frac{u_0 X_0^2}{uX^2}\right)^{\gamma - 1},$$

$$n = n_0 \frac{u_0 X_0^2}{uX^2}$$

and

$$p = p_0 \left(\frac{u_0 X_0^2}{uX^2}\right)^{\gamma},$$

when $(T_e + T_i)_0$, n_0 and p_0, the corresponding boundary values at X_0, are specified. In fact, the temperature–velocity relation gives us the relation between A and a constant parameter A_0, the value of A at X_0, which is used to evaluate the parameter B in the problem. It is noted that the values of pressure and density at a location far away from the black hole, p_0 and n_0, do not affect the flow. They are related to each other for a given temperature, which in turn affects the flow through the parameter A_0.

2.2 Exact solutions and numerical method

The exact solutions to equations (5) and (6) can be found analytically. In the isothermal case ($\gamma = 1$), the solution is

$$1 - \frac{2}{X} + u^2 = \left(\frac{uX^2}{u_0 X_0^2}\right)^{2B} \left\{1 - \frac{2}{X_0} + u_0^2 + v_0^2 \left[1 - \frac{2}{X_0} - \frac{X_0^2}{X^2}\left(1 - \frac{2}{X}\right)\right]\right\} \tag{12}$$

and

$$v = \frac{v_0 X_0}{X} \left(\frac{uX^2}{u_0 X_0^2}\right)^{1/(1+\lambda+c_0)}. \tag{13}$$

If $\gamma \neq 1$, which includes the adiabatic perfect gas case, $\gamma = 5/3$ for a non-relativistic gas, the solution is

$$\left(1 - \frac{2}{X} + u^2\right)\left[(\lambda+1)(uX^2)^{1-\gamma} + \frac{1}{A_0 (u_0 X_0^2)^{\gamma-1}}\right]^2 = \left(\lambda + 1 + \frac{1}{A_0}\right)^2 (u_0 X_0^2)^{2(1-\gamma)} \times \left\{1 - \frac{2}{X_0} + u_0^2 + v_0^2 \left[1 - \frac{2}{X_0} - \frac{X_0^2}{X^2}\left(1 - \frac{2}{X}\right)\right]\right\} \tag{14}$$

and

$$v = \frac{v_0 X_0}{X} \frac{(\lambda+1)(u_0 X_0^2)^{1-\gamma} + c_0}{(\lambda+1)(uX^2)^{1-\gamma} + c_0}, \tag{15}$$

where

$$c_0 \equiv \frac{1}{A_0 (u_0 X_0^2)^{\gamma-1}}. \tag{16}$$

When $v_0 = 0$, the above solutions reduce to the radial relativistic accretion flows (cf. Shapiro & Teukolsky 1983).

Actually, the exact solutions (12), (13), (14) and (15) may be rewritten into conservative forms. A universal form valid in both isothermal and adiabatic situations is

$$\frac{vX}{\sqrt{s^2 + s^2 v^2 + u^2}} = \frac{v_0 X_0}{\sqrt{s_0^2 + s_0^2 v_0^2 + u_0^2}} \equiv l, \tag{17}$$

where $s^2 \equiv 1 - 2/X$. It is very easy to understand the above equation by using proper measurements. In the proper frame, the angular velocity is

$$v^{\mathrm{p}} = \frac{sv}{\sqrt{s^2 + s^2 v^2 + u^2}}, \tag{18}$$

and the proper distance $X^{\mathrm{p}} = X/\sqrt{1 - 2/X}$. Therefore one may write $l = X^{\mathrm{p}} v^{\mathrm{p}} =$ constant, which is simply the law of conservation of angular momentum per unit mass in the proper frame.

With the help of l, the exact solutions (12) and (14) can be rewritten, respectively, as

$$\frac{(s^2 + u^2)(uX^2)^{-2B}}{1 - s^2 l^2/X^2} = \frac{(s_0^2 + u_0^2)(u_0 X_0^2)^{-2B}}{1 - s_0^2 l^2/X_0^2} \equiv E \tag{19}$$

for the isothermal case, and

$$\frac{(s^2 + u^2)}{(1 - s^2 l^2/X^2)(1 - B\lambda)^2} = \frac{(s_0^2 + u_0^2)}{(1 - s_0^2 l^2/X_0^2)(1 - B_0\lambda)^2} \equiv H^2 \tag{20}$$

for the adiabatic case.

From the above discussion, we find that l can be considered as another parameter, and v can be calculated from u and l by algebraic equations. It is found that, according to

equation (17),

$$v^2 = l^2(s^2+u^2)/(X^2 - l^2 s^2). \quad (21)$$

Therefore we only have one ODE to be solved. To put it in another way, one may easily calculate the azimuthal velocity according to equation (21) when u is known. Only the equation governing u needs to be solved to find all the solutions.

Although the closed forms of the solutions have been obtained, the majority of the work that follows relies on obtaining numerical solutions. First, the exact solutions (12) and (14) only give the implicit relation between u and X, and no explicit function $u(X)$ can be found. Therefore, for given boundary conditions and parameters, the exact solution $u(X)$ can be obtained only through numerical solutions of the algebraic equations (12) and (14). Actually, when a solution in a certain range of X is needed, the numerical integration of the ordinary equations may be more economical than the numerical algebraic solution based on the exact solution formula. Secondly, this work is the first part of a series of papers addressing accretion problems including viscosity and θ-dependence, for which a closed form of the solution is very unlikely to be found, or even to exist, and therefore the numerical integration of the basic equations becomes essential. For these various reasons, the solutions to equation (5) are mainly obtained by numerical integrations. However, the analytical results (or numerical solution of algebraic equations 12 and 14) are used to provide comparison with the numerical solution (or numerical integration of the governing equations). They also provide us with guidance in choosing appropriate parameters and boundary conditions.

To carry out the numerical simulation, one first needs to determine a computational domain. For the accretion flow far away from the black hole, gravity is weak and the velocity is low, and therefore the relativistic effects can be ignored. The steady solution for the resultant Newtonian flow is $p = p_\infty$, $n = n_\infty$, $(T_e + T_i) = T_\infty$, $u = C_1/X^2$ and $v = C_2/X$, where C_1 and C_2 are constants. The asymptotic solutions are useful in determining the boundary locations. We choose our boundary position at X_0 as long as the condition

$$\left| \frac{uX^2]_0 - uX^2]_\infty}{uX^2]_\infty} \right| < \Delta$$

is satisfied, where Δ is a given small number (say ~ 1 per cent). For most of the cases, we integrate the governing equation from X_0 to $X = 2$, the location of the event horizon for the Schwarzschild metric.

2.3 Flow pattern and sonic point

Since equation (5) is of the form N/D, the signs of N and D determine the sign of $\mathrm{d}u/\mathrm{d}X$. As a result, they control whether u grows or decays with X. Fig. 1 shows a typical example of the flow pattern obtained from the numerical solutions. In this example, the parameters are $\gamma = 1$, $\lambda = 3/2$, $A_0 = 0.1$ and $l = 0$. The different lines correspond to different boundary conditions u_0 at X_0. The solutions to equation (5) could be divided into two unique curves (I and II) and four regions (III, IV, V and VI) with different families of curves. The other two curves representing $N = 0$ and $D = 0$ play an important role in understanding the flow and are plotted by dashed lines. The near-horizontal dashed line is the line for which $D = 0$. It is not a straight line as in Newtonian model (Frank, King & Raine 1992). Below this line, $D < 0$; above it, $D > 0$. The other dashed line (near-vertical) is the line for which $N = 0$ (not the vertical locating X_s). Again, it is not straight. On the left side of the line, $N < 0$; on the right, $N > 0$.

Before discussing acceptable solutions, one should establish what kind of solution is physically expected. For gas accretion on to black holes, far away from the black hole, the accretion velocity should be small, i.e. $u \ll 1$ as $X \to \infty$. Near the black hole, the accretion velocity is comparable to the speed of light, therefore $u \sim 1$ when $X \to 2$.

In region III, D never changes sign ($D < 0$) but N does. As X decreases, u first increases, when $N > 0$, and then decreases, when $N < 0$. The u-solutions in this region yield $u \ll 1$, both far away from and near the black hole. Similarly, in region IV, the values of u change from asymptotically large values far away, say $u \geq 0.5$, to other large values near the event horizon ($u \sim 1$). The solutions in region III are unphysical because they would represent a zero velocity at $X = 2$ (wind-like solutions which cannot occur at the Schwarzschild boundary). Solutions in region IV are physical but they represent very high velocities at the outer boundary point, $X \to \infty$, and are therefore unlikely to occur in nature. In regions V and VI, there exist points such that $D = 0$, $N \neq 0$. At these points, the values $\mathrm{d}u/\mathrm{d}X$ are infinite. They are singular points, and the solutions are therefore unphysical.

There are two special solutions, represented by the curves labelled I and II. Both solutions pass the critical point at which $D = 0$ and $N = 0$. Since both D and N are zero there, the limits of $\mathrm{d}u/\mathrm{d}X$ may be finite. When $D = 0$, $u^2_{D=0} = Bs^2/(1-B)$. If we measure the radial velocity in a corotating frame, the value is

$$\hat{u}^2 = \frac{u^2}{s^2 + u^2}. \quad (22)$$

Putting $u_{D=0}$ in, we obtain $\hat{u}^2_{D=0} = B$. The radial velocity measured in the corotating frame equals the sound speed when $D = 0$. We can also show that $\hat{u}^2 > B$ when $D > 0$, and $\hat{u}^2 < B$ when $D < 0$. Therefore the flow with $D > 0$ represents supersonic flow, the flow with $D < 0$ represents subsonic flow, the critical point represents the sonic point and the two special solutions (I and II) represent transonic solutions. As X decreases from an asymptotically large value to $X = 2$, curve II is a solution from supersonic to subsonic. The values of u are, correspondingly, large far away and small near the black hole, and would correspond to a wind, and therefore unphysical, solution for accretion on to a black hole. The other transonic solution, represented by curve I, is a solution from subsonic to supersonic. The values of u are small at large X, and large (near unity) as X approaches 2. This is exactly the unique solution representing gas accretion on to the central black hole.

We now focus on the physical transonic solution represented by curve I. As shown in Fig. 1, for a given set of parameters λ, γ, A_0 and l, there is only one value of u_0 from which the expected transonic solution may be obtained. Therefore a search is needed to find this particular solution. The exact analytical solution can be used to guide this search. Given the values of other parameters and X_0, the initial condition u_0, from which the transonic solution can be obtained, and the sonic point position X_s can be calculated through the analyti-

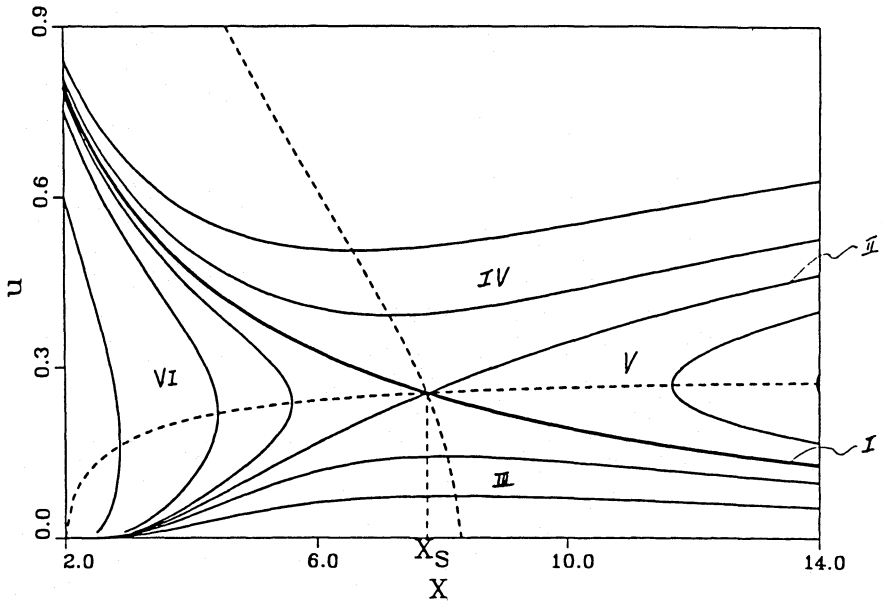

Figure 1. Flow pattern, with parameters $A_0 = 0.1$, $\gamma = 1$, $\lambda = 1.5$ and $v = 0$.

cal solution and conditions $D = N = 0$. This process also provides a verification method for the overall numerical solutions.

The sonic points may not be unique in the accretion flows (Abramowicz & Zurek 1981; Lu 1985). Lu (1985) has shown that, for adiabatic flow with $\lambda = 3$, there is non-uniqueness when the specific enthalpy at infinity H is less than the critical value $H_{crit} \approx 1.02$. For the adiabatic hot-disc flow discussed here, the values of H are much larger than the critical value. In the cool adiabatic case, $\lambda = 1.5$, for which the sonic point is always unique for any given angular momentum. Therefore, for the adiabatic flows investigated here, the sonic points and the transonic solutions are always unique.

In the isothermal cases, we can follow a similar route to find, analytically, the X_s–l relations, with the square of sound speed (B = constant) as a parameter. For $B < B_c = 0.017\,548$, there exists a range of angular momenta l, in which there are three critical points. In this case, we use l'Hopital's principle to evaluate the value of N/D at the critical points. It is found that, at the middle sonic point, N/D has a complex value, which is unphysical. At the other two points, N/D has two real values at each location. One of the X-derivatives of u is negative, which corresponds to the accretion flow. We may use the information obtained here to start the numerical integration from a point very close to the critical point. We use this method only in discussing some special properties. In most of the numerical simulations, we zero in to the transonic solution by integrating the ODE from X_0 to $X = 2$.

3 RESULTS

3.1 Hot accretion flows

For hot discs, $(T_e + T_i)_0 \sim 10^{11}$–$10^{13}$ K or $A_0 = 10^{-2}$ to 1, $\lambda = 1.5$–3, and $\gamma = 1$ in the isothermal case or $\gamma = (\lambda + 1)/\lambda$ if the gas is adiabatic. The boundary conditions are assumed values of u_0 at X_0 large, say $X_0 = 200$, and for a given angular momentum l. As we mentioned before, for each given value of l, there is only one value of u_0 from which the transonic solution can be obtained. In other words, there is a functional relation between u_0 and l, say $u_0 = f(l)$, and, by satisfying this, one may find the transonic solution from subsonic to supersonic. The relation $f(l)$ is implicitly given by the solutions and the critical conditions $D = N = 0$. In practice, we first assume a value of l and then search for u_0, such that the solution is transonic from subsonic to supersonic. We assume here the hottest possible discs, $(T_e + T_i)_0 \sim 10^{13}$ K, $A_0 = 1$, $\lambda = 3$, and $\gamma = 1$ (isothermal) or $\gamma = 4/3$ (adiabatic).

Fig. 2 shows the u-distribution in the X–l plane for the isothermal case. For all ranges of l, u is a monotonic function of X. The crosses denote the sonic points, X_s, for each l value. It is found that the locations of the sonic points, and the corresponding velocities at the sonic points, are not very sensitive to the value of angular momentum. They are all located close to the black hole boundary ($X_s \sim 3$–4). Since the initial values of the state variables at $X_0 = 200$ are the same, the accretion rate $(n_0 u_0 X_0^2)$ is proportional to the velocity u_0. Accordingly, Fig. 2 shows that the accretion rate decreases with the angular momentum as is physically expected.

The results for the adiabatic case are shown in Fig. 3. The u–X–l relations are qualitatively the same as those in the isothermal case. The variations of X_s and the accretion rate with l follow the same trend in both isothermal and adiabatic situations, but their rates are quantitatively different. As the angular momentum increases, the location of the sonic point moves toward the event horizon. Roughly speaking, the distance between the black hole and the sonic locations decreases more rapidly in the isothermal case than in the adiabatic case. In other words, the locations of the sonic

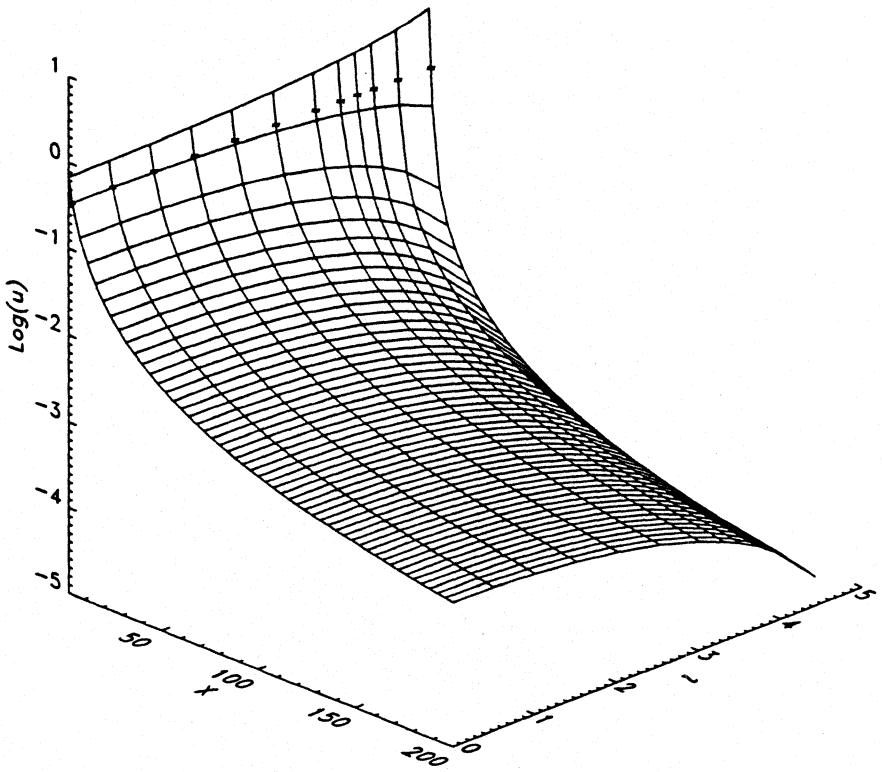

Figure 2. The u–X–l relation in isothermal hot disc accretion, with parameters $A_0 = 1$, $\gamma = 1$ and $\lambda = 3$.

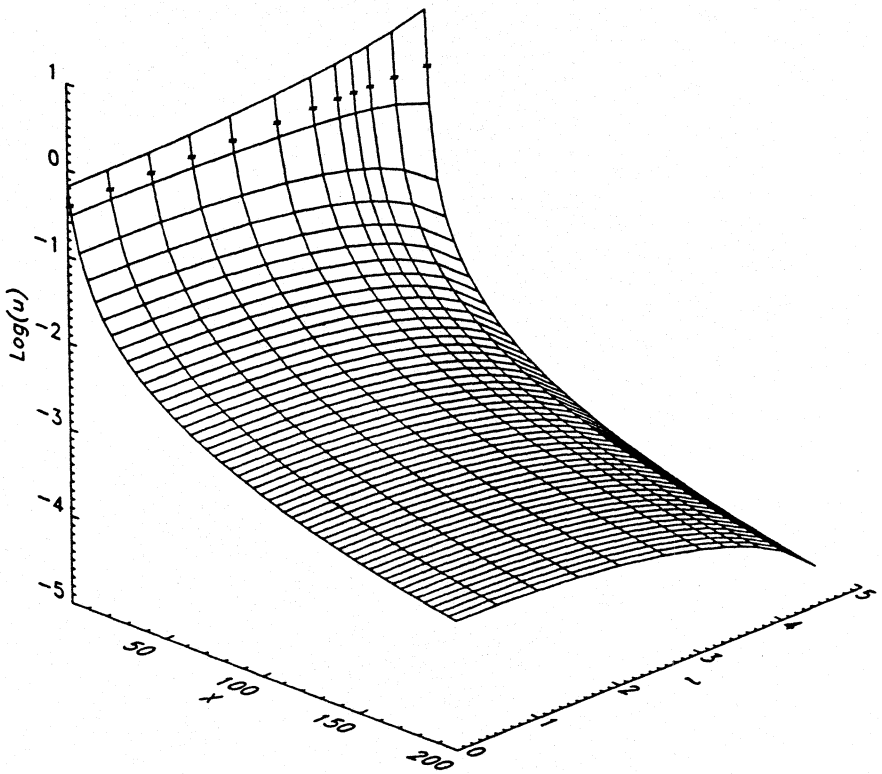

Figure 3. The u–X–l relations in adiabatic hot disc accretion, with parameters $A_0 = 1$, $\gamma = 4/3$ and $\lambda = 3$.

points are more sensitive to the value of the angular momentum in the isothermal case than they are in the adiabatic case.

It is easy to find, from equation (21), that $v \sim l/X$ for large X. The numerical solutions demonstrate that the approximation is also valid for other ranges of X. For this reason, the v–l–X relations are trivial and the corresponding numerical results are not shown here.

An interesting phenomenon is the dependence of the accretion rate on l, which is plotted in Fig. 4. Here we use $R_0 \equiv u_0 X_0^2$ to represent the accretion rate when n_0 is taken as a constant for different l-values. The dashed curve represents the isothermal case ($\gamma = 1$), while the solid curve corresponds to the adiabatic case ($\gamma = 4/3$). When $l = 0$, the value of R_0 in the isothermal case is larger than that in the corresponding adiabatic case. As l increases, the value of R_0 decreases more quickly in the isothermal case than it does in the adiabatic case. At one value of l ($l \simeq 3.72$), the value of R_0 in the two cases becomes the same. When l is higher than this value, the accretion rate in the adiabatic case is slightly greater than that in the isothermal case. This result agrees with the temperature distribution, as we will discuss below.

The major difference between the isothermal case and the adiabatic case is, of course, that the temperature in the adiabatic condition is no longer a constant. The T–X–l relation in this case is presented in Fig. 5, where we define $T \equiv (T_e + T_i)/(T_e + T_i)_0$. First, we find that T is close to a constant near $X_0 = 200$. This justifies the statement that, when X_0 is sufficiently large, the flow beyond it is approximately Newtonian. The temperature increases initially when the gas moves towards the black hole. This trend changes in specific form according to the values of the angular momentum. The temperature keeps increasing for small angular momentum ($l < 3.2$) but begins decreasing for larger l-values, starting at $X \simeq 10$. For even larger values of l (> 3.7), the decrease is so rapid that T is less than unity close to the event horizon. Since $n^{\gamma-1} \propto (T_e + T_i)$, for cases with small l, we can say that u and n increase as X decreases. For the solutions with large l, the increase of u is so large that n must decrease to satisfy the continuity condition ($nuX^2 = $ constant). In other words (from the overall conservation of energy), the gravitational potential energy is transformed to bulk kinetic energy and heat for small-l cases as the gas moves close to the black hole. For large-l cases, near the black hole, the increase in kinetic energy is so rapid that the loss of the potential energy alone is not large enough. The gas would become cooler or lose heat energy in order to compensate for the increase in kinetic energy. Due to this effect, the gas is easier to accrete on to the black hole in the adiabatic case than in the isothermal case for high values of the angular momentum.

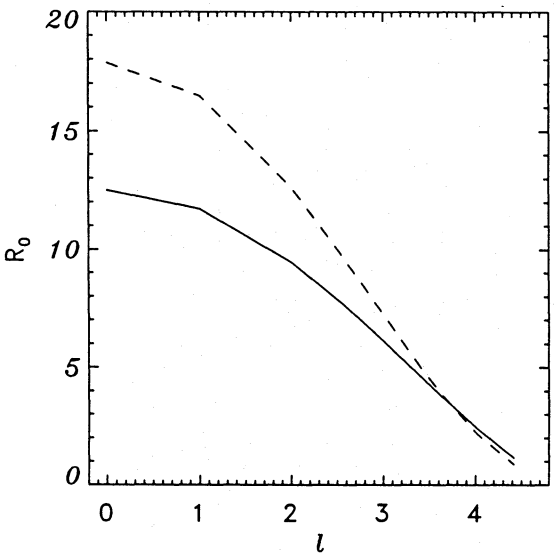

Figure 4. Variation of $u_0 X_0^2$ with l in hot disc accretions, with parameters $A_0 = 1$, $\gamma = 1$ (dashed line) and 4/3 (solid line) and $\lambda = 3$.

As previously mentioned, the sonic points could be calculated analytically, based on the exact solutions (12) and (14). From these solutions, the special values X_s and u_0 could be calculated with an assumed initial X_0-value. Table 1 gives the comparisons of the numerical results with the exact solutions for the $l = 0$ case. The errors for both the sonic point locations X_s and the boundary values u_0 are very small. These can be considered as providing confirmation of the numerical programs, and we conclude that these results verify the validity of our numerical solutions.

The values of Δ defined in Section 2.2 can be estimated after the numerical solution is known. It is found that, at the same location X_0, the value of Δ takes its maximum when $l = 0$, and in the isothermal case. For this reason, we choose the Δ-value under isothermal conditions and with $l = 0$, to judge the validity of the assumed value of X_0. For the hot disc discussed here, Δ is found to be less than 0.5 per cent at $X_0 = 200$. Therefore we say that $X_0 = 200$ is sufficiently large (beyond that value the solution is close enough to the Newtonian solution) for studying the problems given here.

We have made a comparison between the critical accretion rate and the accretion rate obtained here under certain circumstances ($n_\infty \sim 10^9$ cm^{-3} for supermassive black holes and 10^{16} cm^{-3} for stellar black holes). The ratio of $\dot{M}/\dot{M}_{\rm Edd}$ obtained is about 1 per cent, a reasonable value.

3.2 Single-temperature accretion flows

After studying the hot disc accretion, it is natural to do a similar study for cooler discs, where $(T_e + T_i)_0 \sim 10^9$ K, and $A_0 \sim 10^{-4}$. In this case, the parameter λ is 3/2, $\gamma = 1$ in the isothermal condition and $\gamma = 5/3$ in the adiabatic condition. It can then be shown that $X_s \sim A_0^{-1}$ in the isothermal condition, and a much larger spatial range must be covered in the numerical computation than was previously done for the hot disc accretion.

In a specific example solved here, the parameter A_0 is set to be 2×10^{-4}, corresponding to $(T_e + T_i)_0 \sim 2 \times 10^9$ K. If the electrons and protons are in thermal equilibrium, it is generally expected that the electrons will cool the disc to $\sim 10^9$ K. Higher values of T_e would result in catastrophic e^+e^- pair production (Kusunose & Takahara 1985). Hence cooler discs, for which $T_i \sim T_e$, are in general physically allowed cases if $T_e \sim 10^9$ K (Novikov & Thorne 1973). The boundary is chosen at $X_0 = 5000$, at which point the estimate on Δ is about 0.013 ($l = 0$ and $\gamma = 1$). It may not actually be possible to sustain 10^9-K temperatures out to that distance (Novikov & Thorne 1973), but we proceed as if this was possible in order to analyse the numerical results for finding the sonic

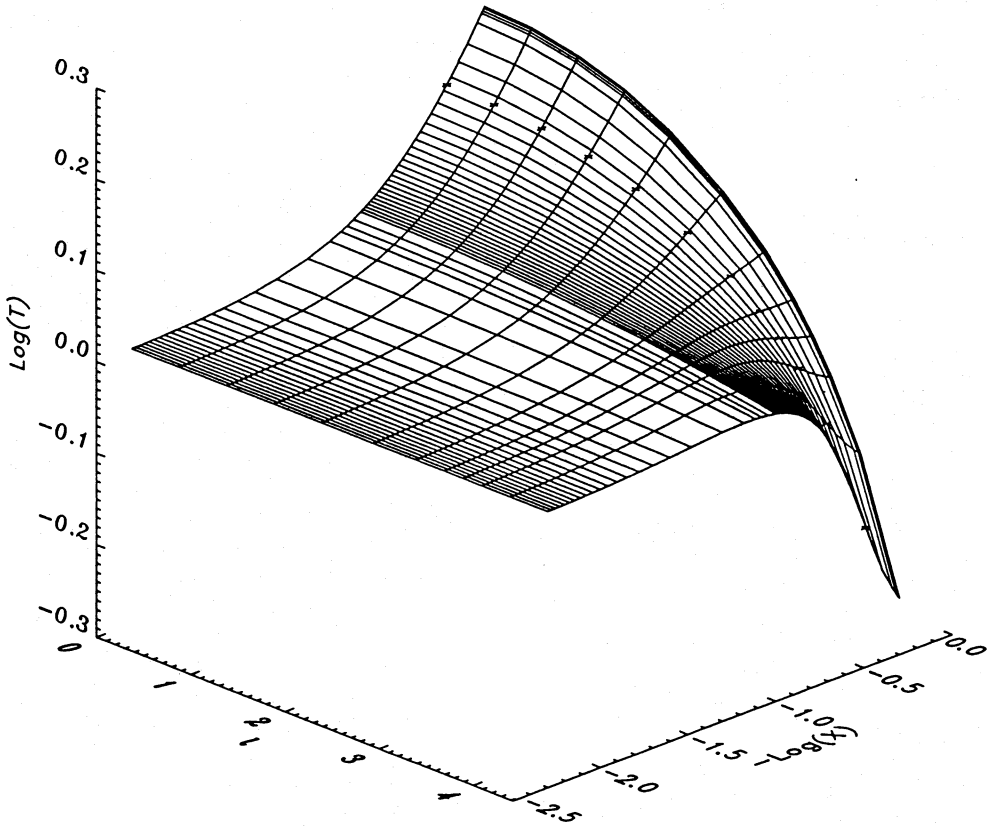

Figure 5. The T–X–l relation in adiabatic hot disc accretion; the parameters are the same as those in Fig. 3.

Table 1. Comparison of the exact and numerical values in the hot disc. The index 'n' represents the values from numerical solution, and 'a' denotes the analytical values.

			$A_0 = 1$, $\lambda = 3$			
γ	X_{sn}	X_{sa}	Error	u_{0n}	u_{0a}	Error
4/3	3.265	3.260	0.00155	0.0003125	0.0003124	0.00002
1	4.008	4.000	0.00200	0.0004466	0.0004465	0.00019

point, which may lie at a location far away from the black holes and, therefore, outside a physical accretion disc.

Fig. 6 shows the u–X–l relations for the transonic solutions in the adiabatic case. As a whole, this flow is qualitatively the same as that in the hot adiabatic condition. One significant difference is the order of the sonic points and their dependence on l. In the cool case, the sonic point location X_s decreases from about 54, when $l=0$, to 4, when l approaches 4. Moreover, the value of u at the sonic point, u_s, varies in a non-monotonic way as l increases. Initially, it increases with l for small values of l, and then it decreases for large values of l. By contrast, in the hot disc, u_s decreases always with increasing values of l.

Fig. 7 shows the u–X–l relations in the isothermal case. It is noted that the behaviour of the radial velocity is similar to that in the hot disc case at small values of l ($l<3$). In this range of l, the locations of the sonic points are very far away from the black hole, and their velocities at these points are almost constant. Since X_s is relatively large, $(1-2/X)\sim 1$, the sonic condition $D=0$ (equation 8) leads to

$$u_s^2=\frac{B}{1-B}\left(1-\frac{2}{X_s}\right)\sim\frac{B}{1-B}.$$

In the isothermal case, $\gamma=1$, equation (11) gives $B=1/(1+\lambda+A_0^{-1})$, a constant, and hence u_s is approximately a constant. Actually, in this case, $A_0\ll 1$, hence $B\sim A_0$ and $u_s^2\sim B$. The approximate value of u_s is 0.0141, which is exactly the same as those obtained from the numerical solutions to three-digit accuracy. It should be pointed out that this estimate is possible only when X_s is known to be large.

For flows with larger l-values, u is no longer a monotonic function of X. The explanation for this is as follows: for the cooler disc case, the values of A_0 and consequently the values of B are very small. According to equation (7), the dependence on the v-value is very important in evaluating N in this condition. As shown in Fig. 1, the supersonic part of the transonic solution is achieved under conditions $D>0$, $N<0$ and $\mathrm{d}u/\mathrm{d}X<0$. Since the value of v rises as the gas accretes on to the black hole, as implied by equation (21), at some point, the value of v becomes so large that the value of N increases to zero from a negative value near the sonic point. A further increase of the v-values makes the values of $\mathrm{d}u/\mathrm{d}X$ positive. As a consequence, the value of u drops as X decreases. Other terms in N will make N become negative again for some smaller X. The effect of N is demonstrated in

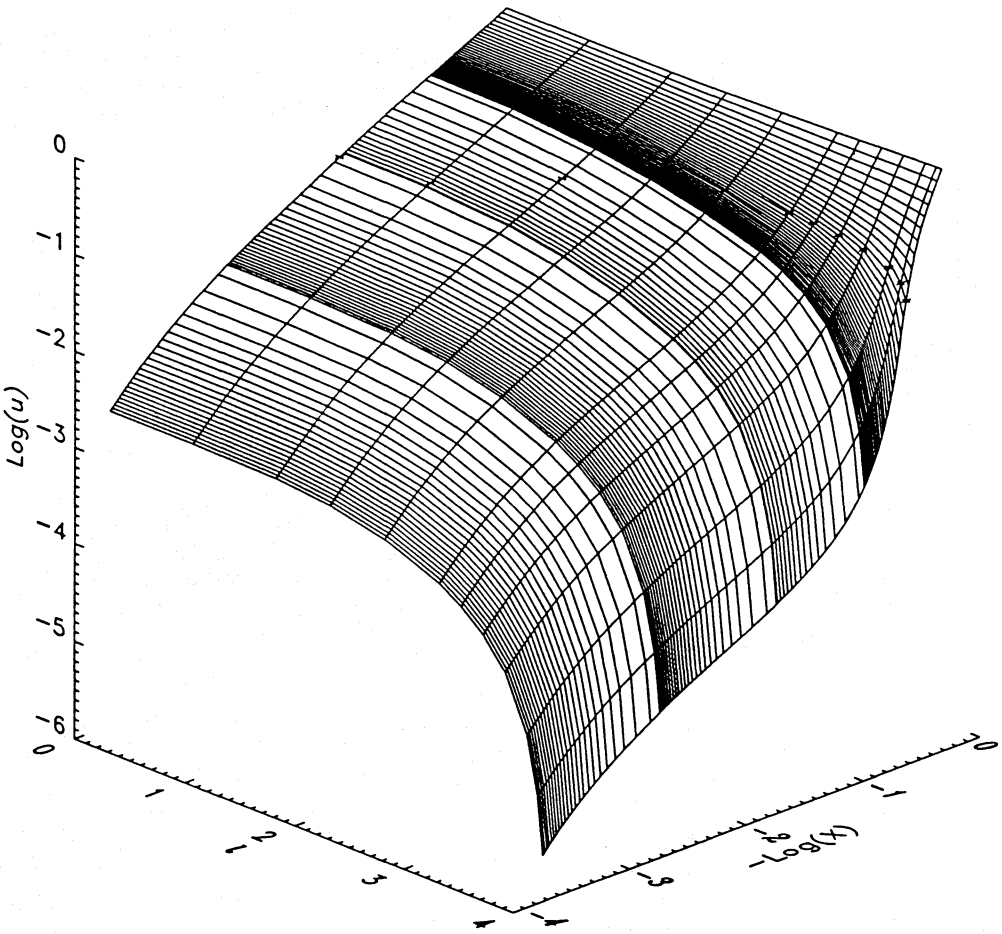

Figure 6. The u–X–l relation of the transonic solutions in adiabatic cold-disc accretion flow, with parameters $A_0 = 0.0002$, $\gamma = 5/3$ and $\lambda = 1.5$.

Fig. 8, which is similar to the flow pattern in Fig. 1. Here, only the transonic solutions are plotted. The corresponding angular momentum has values $l = 3.60$ and $l = 3.985$, respectively. The dot-dashed line represents the $D = 0$ curve, which is independent of l. The $N = 0$ curves are plotted by the dotted line ($l = 3.60$) and the dashed line ($l = 3.985$). This figure clearly shows that the curve of $N = 0$ has a local valley, and that the depth of the valley increases with the angular momentum. When the transonic solutions are located in the valley, $\mathrm{d}u/\mathrm{d}X > 0$, since $N > 0$ and $D > 0$. That is why the u–X solution is not monotonic in this region. For large l-values, this valley is so deep that the $N = 0$ curve will touch the $D = 0$ curve at two more points. As a matter of fact, in this special situation, the sonic point is not unique. We will study the case of multiple sonic points in detail in the next section.

Once again, we calculate analytically the values X_s and u_0 for the $l = 0$ case and compare the result with the numerical solution. Table 2 lists the values we obtained from both numerical and analytical solutions. The relative errors of the numerical solution are, again, very small.

Compared with the hot disc accretion, the assumption of thermodynamic conditions, isothermal or adiabatic, has a strong effect on the location of the sonic point in a cool disc. The distance between the sonic point and the event horizon in the isothermal case is two orders of magnitude larger than the corresponding distance in the adiabatic case when l is small.

3.3 Unique transonic solution with multiple sonic points

As stated earlier, when $B < B_c$, there is a range of l in which there exist two possible sonic points. We will call them the inner sonic point and the outer sonic point, according to their distances from the black hole. In order to investigate clearly the accretion flow in the case of multiple sonic points, we choose $A_0 = 0.006$ ($B = 0.005\,9113$), which corresponds to $(T_e + T_i)_0 \sim 6 \times 10^{10}$ K, since the special properties are easily studied for this parameter.

With the known possibility of multiple sonic points, we still use the zeroing, or shooting, method to search the transonic solutions, starting from $X_0 = 200$. In this case, we only want to study the effect of multiplicity of sonic points, and no estimate of Δ is given. The result is shown in Fig. 9 by the u–X–l relation. From the previous work, the multiplicity appears only for a range of l-values, say $l_A < l < l_B$ (Abramowicz & Zurek 1981). For our case, with $A_0 = 0.006$, we find that $l_A = 3.595$ and $l_B = 4.944$. There is another special value

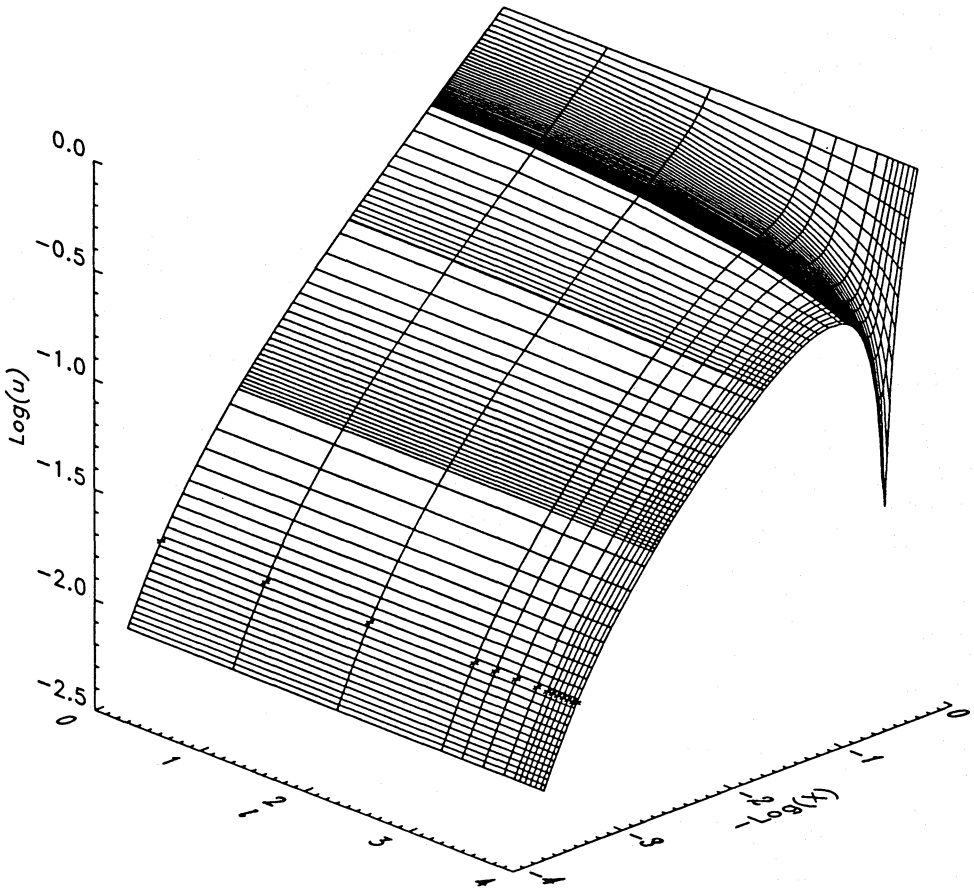

Figure 7. The u–X–l relation of the transonic solutions in isothermal cold disc accretion, with parameters $A_0 = 0.0002$, $\gamma = 1$ and $\lambda = 1.5$.

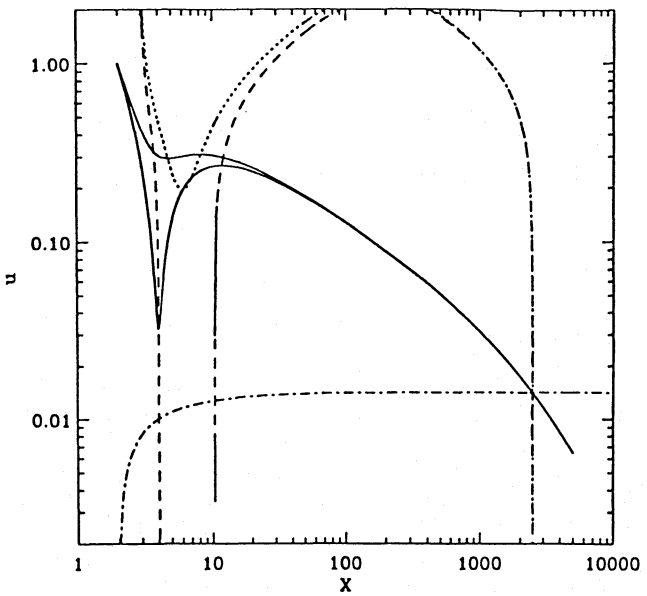

Figure 8. The u–X relations of the transonic solutions and the relations governed by $D = 0$ and $N = 0$ in isothermal cold disc accretion. Solid lines: transonic solutions; dashed line: $N = 0$ curve, when $l = 3.60$; dotted line: $N = 0$ curve, when $l = 3.985$; mainly horizontal dot-dashed line: $D = 0$ curve. (Note that the mainly vertical dot-dashed line on the right of the figure is a superimposition of the dotted and dashed lines.) Parameters are $A_0 = 0.0002$, $\gamma = 1$ and $\lambda = 1.5$.

of l, l_M, which separates the monotonic u–X relation and non-monotonic u–X relation due to the change of sign of N, when l crosses l_M, as described in the last section. The l_M-value found here is about 2. When $l < l_A$, the transonic flow passes the unique sonic point and the u–X relation is monotonic for $l < l_M$ but non-monotonic for $l > l_M$. When l is slightly higher than l_A, the transonic solution passes the outer sonic point with a stronger non-monotonic effect between u and X. The region with decreasing u becomes larger, and the local minimum u becomes smaller, as l increases. This process can continue until l reaches a critical angular momentum l_C, at which the local minimum of u takes place at the inner sonic point. In this special situation, the transonic solution can pass both the outer and the inner sonic points. When $l > l_C$, the transonic solution passes only the inner sonic point. The non-monotonic part of the u–X relation is in the subsonic region. In other words, when l continuously varies across l_C, the sonic point reached by the transonic solutions has a jump between the outer sonic point and the inner sonic point. The theoretical value for l_C is found to be 3.7677. The two close solutions that show the jump of sonic points in Fig. 9 have l-values of 3.767 and 3.769, respectively.

Although the sonic point jumps as l increases, to cross a special value l_C, the accretion rate ($\propto u_0$) is continuous, as shown in Fig. 9. Moreover, when the flow passes the outer

sonic point, the accretion rate remains almost constant. When the solution passes the inner sonic point at a high angular momentum, however, the accretion rate decreases very quickly with l. If we assume that the solution passing the inner sonic point and the solution passing the outer one are two different branches of the transonic solutions, our numerical shooting method automatically chooses a solution with lower accretion rate, as proved by Lu & Abramowicz (1988), in the adiabatic case. If we use the energy E, defined by equation (19), instead of the accretion rate, it is found that the unique solution corresponds to the branch of higher energy. In order to prove that the solutions shown in Fig. 9 are unique, we use the N/D values from the theoretical analysis to start the numerical integration from the sonic points. That is, for $l < l_C$, we start from the vicinity of the inner sonic point and integrate outwards; for $l > l_C$, we start from the vicinity of the outer one and march inwards. In both cases, the numerical integration cannot continue at some points, either because u decreases to infinitesimal values or because the singularity is reached ($D = 0$, $N \neq 0$). This result suggests that the solutions passing the inner sonic point when $l < l_C$, and the solutions passing the outer one with $l > l_C$, do not exist for a realistic accretion since it requires that the solutions hold for all ranges of X, from the event horizon to infinity. The accretion flow has a unique transonic solution even though the possible sonic points are multiple.

It should be pointed out that the above discussion is valid for shock-free solutions. A transonic solution may pass both sonic points with a shock between them (Chakrabarti 1990; Yang & Kafatos 1994, in preparation). Chakrabarti & Wiita (1992) have studied the spectra of a specific AGN, based on the standing shock assumption in accretion discs, and found improved agreement. It is expected that, without shocks, the velocity profile shown in Fig. 7 may also improve the spectral estimate, since the drop in the velocity may have a similar effect to the drop resulting from shocks.

Table 2. Comparison of the exact and numerical values in the cool disc.

			$A_0 = 0.0002$,	$\lambda = 1.5$		
γ	X_{sn}	X_{sa}	Error	u_{0n}	u_{0a}	Error
5/3	54.200	54.169	0.00058	0.0017511	0.0017511	0.00000
1	2503.1	2502.8	0.00014	0.00647763	0.00647757	0.00001

3.4 Limits on angular momentum

It is obvious that the accretion rate decreases with the angular momentum in all cases, although the dependence may be

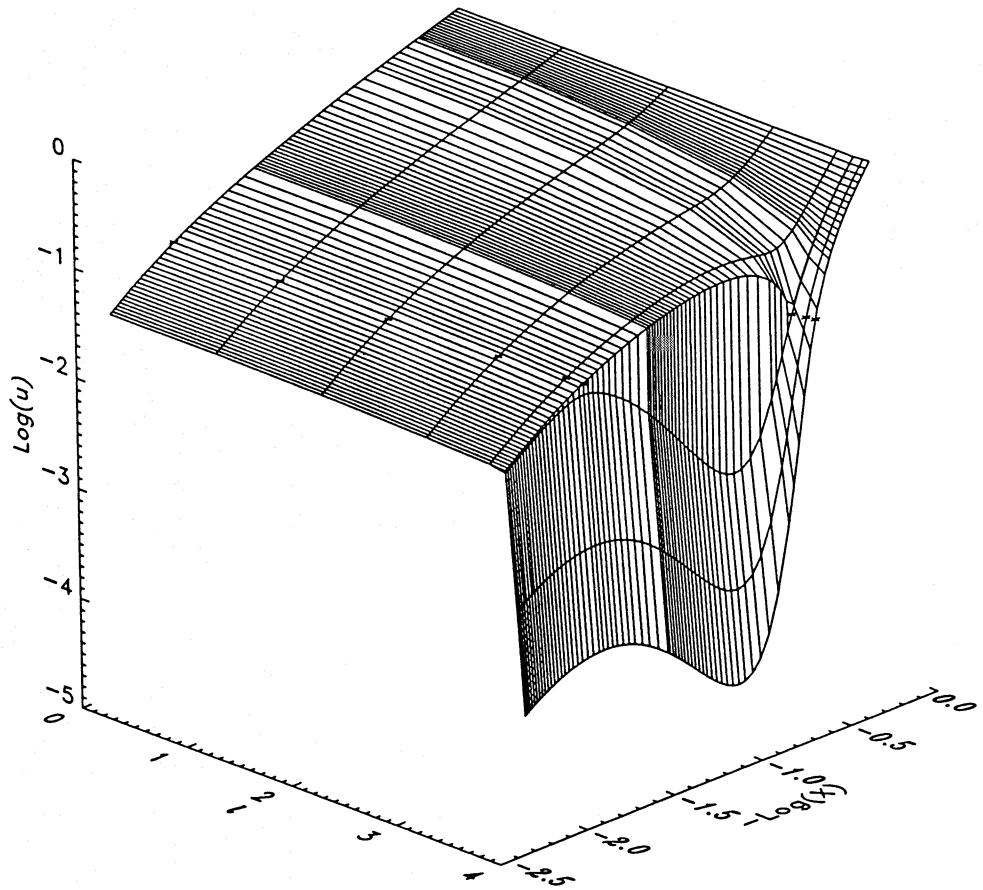

Figure 9. The u–X–l relation of the transonic solutions, which shows the jump between the two sonic points across l_C. Parameters are $A_0 = 0.006$, $\gamma = 1$ and $\lambda = 1.5$.

weak in one circumstance and strong in another. When the angular momentum is large enough, the accretion cannot be sustained, since the centrifugal force and gravity would balance each other at some location.

By setting $u=0$ at the sonic point, and $X_s>3$, we find that, in adiabatic flows, the upper limit of angular momentum $l_u^2=X_s^3/(X_s-2)^2$, with $X_s=(3H^2-4+H\sqrt{9H^2-8})/2(H^2-1)$. Here H, the enthalpy at infinity, is a constant determined by equation (20). This gives a relationship between l and H, which describes the limitation on angular momentum for given H in accretion flows. The result is shown in Fig. 10. There are two special limiting values of l: when $H\rightarrow\infty$, a very hot disc, $X_s\rightarrow 3$ and $l_u^2\rightarrow 27$; when $H\rightarrow 1$, a very cold disc, $X_s\rightarrow 4$ and $l_u^2\rightarrow 16$.

The analytical result can be tested by the numerical simulation. In the hot adiabatic case, the theoretical value is $l_u=5.16$, while our numerical integration can find a transonic solution to a l-value as high as 5.12. In the cool disc case, l_u is found to be 4.00 analytically, while the numerical integration can be run at an angular momentum as high as 3.95. The crosses in the figure denote the upper limits of l found by the numerical shootings.

For isothermal flows, the $(uX^2)^{-2B}$ term in equation (19) prohibits us from doing the same analysis as in the adiabatic case. Our numerical integrations can go as high as $l=5.17$ in the hot isothermal disc ($A_0=1.0$), and $l=3.985$ in cool conditions ($A_0=0.0002$). It seems that the difference between the isothermal condition and the adiabatic condition on providing upper limits to l is not large. It should be noted, however, that $l=5.17$ in the isothermal situation, as obtained from the numerical simulation, is higher than the theoretical value in the adiabatic case. There must be some differences between these two situations. For realistic astrophysical conditions, such as capture of material in a binary orbit for stellar black holes (say with $M\sim 10\ M_\odot$ and orbital periods less than a day), or capture from an interstellar cloud at a capture radius (Shapiro 1973) with characteristic speeds ~ 300 km s^{-1} appropriate for galactic orbital velocities, we find that $l=vX]_\infty$ is several orders of magnitude higher than the limits found here. The gas has too much angular momentum at $r\rightarrow\infty$ to be directly captured, and at least two orders of magnitude of reduction needs to take place. A more appropriate value of l far away can be obtained if one assumes Keplerian motions for which $l_K=\sqrt{X}$. In that case a reduction by a factor of a few (if $X=200$) is needed in order to reach the limits formed here. This would, of course, happen if viscosity were present, a factor which has been ignored in the present treatment.

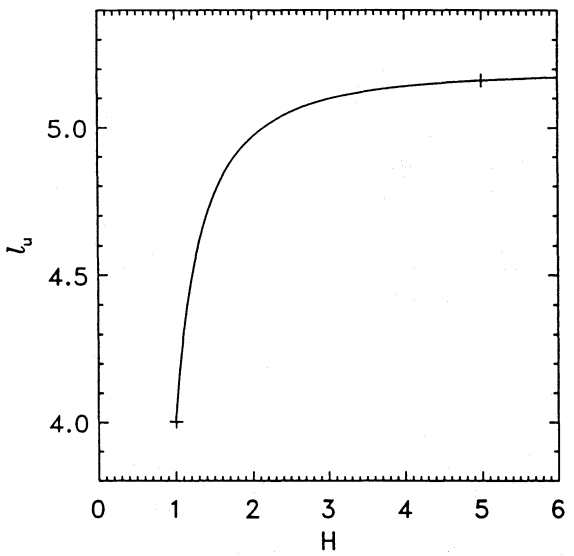

Figure 10. The l_u–H relation. See text for details.

3.5 Comparison with the slim discs

The model studied here is compared with the slim disc model (Abramowicz et al. 1988), as listed in Table 3, in which the standard disc model is included as a reference. The slim disc model works for a disc that has $h/r\leq 1$, and resolves the vertical structure. The model used in this work focuses on a wedge of $h/r=$ constant $\ll 1$ ($\theta\simeq\pi/2$), and therefore it cannot describe the vertical structure. The viscosity is considered in the slim disc by using $\tau_{\varphi r}=-\alpha P$, but here the flow is assumed inviscid. As a result, the angular momentum is conservative in our model but it is not conservative in the slim disc. Moreover, the angular momentum distribution in the slim disc is different from the Keplerian distribution used in the standard thin disc. In the disc models with viscosity (both the standard and the slim discs), the high angular momentum at infinity results in $v_\varphi\gg c_s$ and $v_R\ll c_s$ at infinity. In our model, a relatively small angular momentum is given, and therefore only $v_R\ll c_s$ is required at infinity. The angular momentum in our model may be too small to form accretion discs in certain circumstances, such as the cool isothermal accretion flows passing through the outer sonic points described before. In this case, the transonic flows correspond to the spherical accretion flows.

The accretion rate for the slim disc is about the same as the Eddington accretion rate. Our model would simulate the case of $\dot{M}/\dot{M}_{\rm Edd}\ll 1$. When the ratio $\dot{M}/\dot{M}_{\rm Edd}$ is small in the slim disc, one would find that $h/r\ll 1$, as shown by fig. 8 of Abramowicz et al. (1988).

4 SUMMARY

The accretion flow along the equatorial plane in thin disc flows has been studied both analytically and numerically. The value of the specific angular momentum of the gas, l, has an upper limit in the accretion process. The accretion rate achieves, of course, a maximum value when the angular momentum of the accreting gas is zero. The rate decreases with increasing l-values. In the case of cool isothermal ac-

Table 3. Comparisons among the standard thin disc model, the slim disc model and the model used here.

Model	h/r	Viscosity	l	Radial Velocity	$\dot{M}$
Standard Disk	$\ll 1$	$\tau_{\varphi r}=-\alpha P$	l_K	$v_R\ll C_s$	$\ll \dot{M}_{Edd}$
Slim Disk	<1	$\tau_{\varphi r}=-\alpha P$	$l(r)$	Transonic	$\sim \dot{M}_{Edd}$
Our Model	*const.* $\ll 1$	$\tau_{\varphi r}=0$	l_C	Transonic	$\ll \dot{M}_{Edd}$

cretion, there exist two possible sonic points. The physical accretion flow passing through one of the two points is unique, depending on the value of angular momentum. When the angular momentum varies across the critical point l_C, the flow pattern undergoes a dramatic change, since the transonic solution jumps from the solution associated with one sonic point to the solution associated with the other sonic point. The accretion rate changes continuously across that point, but the variation of the accretion rate with l is much larger for $l > l_C$ than that for $l < l_C$. Single sonic points are found for the other cases examined here, which may be more realistic for the real astrophysical scenario. In subsequent papers, we will examine the effect of motions off the orbital plane as well as a full Kerr metric.

REFERENCES

Abramowicz M. A., Kato S., 1989, ApJ, 336, 304
Abramowicz M. A., Zurek W. H., 1981, ApJ, 246, 314
Abramowicz M. A., Czerny B., Lasota J. P., Szuszkiewicz E., 1988, ApJ, 332, 646
Anderson M., 1989, MNRAS, 239, 19
Becker P. A., Kafatos M., 1994, 2nd Compton Symp., in press
Chakrabarti S. K., 1990, Theory of Transonic Astrophysical Flows. World Scientific, Singapore
Chakrabarti S. K., Wiita P. J., 1992, ApJ, 387, L21
Eilek J. A., Kafatos M., 1983, ApJ, 271, 804
Flammang R. A., 1982, MNRAS, 199, 833
Frank J., King A. R., Raine D. J., 1992, Accretion Power in Astrophysics, 2nd edn. Cambridge Univ. Press, Cambridge
Hartman R. C. et al., 1992, ApJ, 385, L1
Kafatos M., 1988, in Kafatos M., ed., Supermassive Black Holes. Cambridge Univ. Press, Cambridge, p. 307
Kusunose M., Takahara F., 1985, Prog. Theor. Phys., 73, 41
Liang E. P. T., 1979, ApJ, 234, 1105
Liang E. P. T., Thompson K. A., 1980, ApJ, 240, 271
Lightman A. P., Eardley D. M., 1974, ApJ, 187, L1
Ling J. C., Mahoney W. A., Wheaton W. M. A., Jacobson A. S., 1987, ApJ, 321, L117
Lu J. F., 1985, A&A, 148, 176
Lu J F., Abramowicz M. A., 1988, Acta Astron. Sin., 8, 1
Novikov I. D., Thorne K. S., 1973, in DeWitt C., DeWitt B. S., eds, Black Holes. Gordon and Breach, New York/London/Paris
Shakura N. I., Sunyaev R. A., 1973, A&A, 24, 337
Shapiro S. L., 1973, ApJ, 180, 531
Shapiro S. L., 1974, ApJ, 189, 343
Shapiro S. L., Teukolsky S. A., 1983, Black Holes, White Dwarfs, and Neutron Stars. John Wiley & Sons, New York
Shapiro S. L., Lightman A. P., Eardley D. M., 1976, ApJ, 204, 187
Sunyaev R. et al., 1991, A&A, 247, L29
Svensson R., 1984, MNRAS, 209, 175
Thorne K. S., 1981, MNRAS, 194, 439
Thorne K. S., Flammang R. A., Żytkow A. N., 1991, MNRAS, 194, 475
Yang R., Kafatos M., 1994, A&A, submitted